Journal of Catalysis **192,** 355–362 (2000)
doi:10.1006/jcat.2000.2854, available online at http://www.idealibrary.com on IDEAL®

Catalytic Properties and Structure of Zirconia Catalysts for Direct Synthesis of Dimethyl Carbonate from Methanol and Carbon Dioxide

Keiichi Tomishige,[1] Yoshiki Ikeda, Tomohiro Sakaihori, and Kaoru Fujimoto

Department of Applied Chemistry, School of Engineering, The University of Tokyo, 7-3-1, Hongo, Bunkyo-ku, Tokyo 113-8656, Japan

Received October 25, 1999; revised February 16, 2000; accepted February 18, 2000

Selective synthesis of dimethyl carbonate from methanol and CO_2 proceeded effectively on a zirconia catalyst prepared by the calcination of zirconium hydroxide at 673 K. The bulk of this zirconia had a mainly tetragonal structure which was determined by XRD. In contrast, near its surface the monoclinic phase was major and the tetragonal phase was minor, as determined by laser Raman spectroscopy. But the ratio of the tetragonal phase to the monoclinic was higher on this zirconia catalyst than on other catalysts prepared at different calcination temperatures. The number of neighboring acid–base sites estimated by temperature-programmed desorption is suggested to be related to the activity of dimethyl carbonate formation.

1. INTRODUCTION

Dimethyl carbonate (DMC) has attracted much attention as a nontoxic substitute for dimethyl sulfate and phosgene, which are toxic and corrosive methylating or carbonylating agents (1). In addition, DMC is considered to be an option for meeting the oxygenation specifications for transportation fuel (2). Three commercial methods of DMC production have been developed. The first is the stoichiometric reaction of methanol and phosgene,

$$2CH_3OH + COCl_2 \rightarrow (CH_3O)_2CO + 2HCl. \quad [1]$$

The second is the oxidative carbonylation of methanol catalyzed by cuprous chloride in a slurry reaction system (3) where the reaction proceeds in the redox cycle of copper ions as

$$2CuCl + 2CH_3OH + \tfrac{1}{2}O_2 \rightarrow 2Cu(OCH_3)Cl + H_2O, \quad [2]$$

$$2Cu(OCH_3)Cl + CO \rightarrow (CH_3O)_2CO + 2CuCl. \quad [3]$$

A number of patents have been issued on the use of a supported copper catalyst in vapor-phase oxidative carbonylation of methanol (4) in which the most active catalyst was a $[Cu(OCH_3)(pyridine)Cl]_2$ on activated carbon (5).

Recently, the UBE Industry developed an excellent DMC synthesis process using a Pd^{2+} catalyst and an alkyl nitrite promoter (6), which is the third method. The reaction is represented as

$$CO + 2CH_3ONO \rightarrow (CH_3O)_2CO + 2NO. \quad [4]$$

The nonhydrous condition that is realized over the catalyst should contribute to the high catalytic activity being maintained for a long time. The methyl nitrite used in the reaction is synthesized by the following reaction, which proceeds at room temperature without any catalyst:

$$2CH_3OH + 2NO + \tfrac{1}{2}O_2 \rightarrow 2CH_3ONO + H_2O. \quad [5]$$

In the second and third production methods, the raw materials are methanol, CO, and oxygen. In contrast, the utilization of CO_2 as the raw material for DMC synthesis has been attempted. We found that DMC can be synthesized from CH_3OH and CO_2 using CH_3I and K_2CO_3 as the promoters (7). Although this reaction was very fast, the deactivation was very rapid due to the formation of KI. From this study, we found that two functions are necessary for DMC formation: the supply of the methyl species from CH_3I and the basic function for the activation of methanol and CO_2. In direct DMC synthesis from methanol and CO_2, it is important to supply the methyl species from methanol, which can proceed with the acidic function. From this point of view, both acidic and basic functions are necessary for DMC synthesis (6) from methanol and CO_2:

$$2CH_3OH + CO_2 \rightarrow (CH_3O)_2CO + H_2O. \quad [6]$$

Some catalysts have been reported to be effective for the synthesis of DMC from methanol and CO_2. DMC has been synthesized from carbon dioxide and methanol in the presence of organotin compounds (8), Sn(IV) and Ti(IV) alkoxides, and metalacetates (9). Recently, we reported that DMC was selectively synthesized from methanol and CO_2

[1] To whom correspondence should be addressed. Fax: +81-3-5841-8578. E-mail: tomi@appchem.t.u-tokyo.ac.jp.

0021-9517/00 $35.00

using a ZrO_2 catalyst. It was also reported that dimethyl ether (DME) was formed on various oxide catalysts (SiO_2, Al_2O_3, TiO_2, H-ZSM5, H-USY, H-mordenite, ZnO, MoO_3, and Bi_2O_3) and DMC formation was not observed at all (10). It was found that the DMC formation rate was strongly dependent on the structure of zirconia. On zirconia prepared by the calcination of zirconium hydroxide at 673 K, the highest rate of DMC formation was observed (10).

In this paper, we characterized zirconia calcined at various temperatures by thermogravimetric and differential thermoanalysis (TGA-DTA), BET, X-ray diffraction (XRD), laser Raman spectroscopy (LRS), diffuse reflectance infrared Fourier transform spectroscopy (DRIFT), and $CO_2 + NH_3$ temperature-programmed desorption (TPD) to make clear the relation between the catalytic properties and the catalyst structure.

2. EXPERIMENTAL

2.1. Preparation of Catalyst

Zirconia catalysts were prepared by calcining a commercially available $ZrO_2 \cdot xH_2O$ (Nakarai Tesque Inc.) at different temperatures (388–1073 K) for 3 h in air. Catalysts were used in the form of fine powder.

2.2. DMC Synthesis from Methanol and CO_2

The reaction was carried out in a stainless steel autoclave reactor with an inner volume of 70 or 30 ml. The standard procedure is as follows: 6.1 g of methanol (192 mmol, Kanto Chemical, 99.8% minimum) and 0.5 g of catalyst (4.1 mmol) were put into an autoclave, and then the reactor was purged with CO_2. After that, CO_2 (200 mmol, Takachiho Trading Co., Ltd, 99.99%) was introduced into the autoclave at initial pressure about 5 MPa at room temperature. The reactor was heated and magnetically stirred constantly during the reaction. The reaction was carried out at different temperatures (413–463 K) for different reaction times (1–16 h). The products in both the gas phase and liquid phase were analyzed with a gas chromatograph equipped with a FID and a TCD detector. The products were also identified by GC-MS. In the gas phase, almost no products were observed. CO was below the detection limit of GC with the FID detector equipped with a methanator. Under all the reaction conditions shown in this article, DMC was the only product and DME, which is the expected by-product, was below the detection limit of the FID-GC.

2.3. Catalyst Characterization

The XRD spectra and the BET surface area were measured by a RINT-2400 (Rigaku) and Gemini (Micromeritics, N_2) respectively. The amount of CO_2 and NH_3 adsorption was measured by a volumetric method using a vacuum line, which has 30-cm^3 dead volume. The sample pretreatment was evacuation at the calcination temperature for 0.5 h. The pressure of the gas phase at the equilibrium state was about 6.6 kPa of CO_2 and NH_3. Adsorption was carried out at room temperature. Temperature-programmed desorption (TPD) profiles of CO_2 and NH_3 were obtained by the mass spectrometer (Balzers, Prisma QMS 200). Mass signals of $m/e = 44$ and 16 were monitored in the CO_2 and NH_3 TPD, respectively. Sample pretreatment and gas adsorption were performed in a closed circulating vacuum system. In the experiment with CO_2 and NH_3 coadsorption ($CO_2 + NH_3$), CO_2 was introduced into the sample and evacuated, and then NH_3 was introduced. Reverse order of the gas introduction ($NH_3 + CO_2$) was also carried out. Before the measurement of TPD profiles, the sample was evacuated for 1 h at room temperature. The sample weight was 0.05 g. The heating rate was about 7 K/min. NH_3 (99.999%) and CO_2 (99.99%) were purchased from Takachiho Trading Co., Ltd., and they were used without further purification.

Thermogravimetric and differential thermal analyses (TGA and DTA) were performed using a TGD-7600 (ULVAC, Shinku-riko, Inc.). A platinum basket was used as a sample holder and the samples were about 11 mg of $ZrO_2 \cdot xH_2O$. The reference compound in DTA measurement was α-Al_2O_3. TGA and DTA profiles were measured in the air flow (20 ml/min) at a heating rate of 6 K/min.

Raman spectra of the samples were obtained by LABRAM 1B (JOBIN-YVON, He–Ne laser source) in air. Diffuse reflectance infrared Fourier transform spectra were obtained with a Magna 550 (Nicolet) with a MCT detector. An *in situ* cell (Spectra Tech) was used for high-temperature and high-pressure observation. Catalyst powder was put in the sample cup in the cell. This cell was connected to the high-pressure gas flow system. Methanol was introduced by the pulsed gas at atmospheric pressure with He as the carrier gas until the coverage reached the saturation level. The sample temperature was kept at 443 K. Pretreatment was carried out by He flow at the same temperature as the calcination for 0.5 h. The spectra were obtained 10 min after introduction of the methanol and CO_2.

3. RESULTS AND DISCUSSION

3.1. DMC Synthesis from Methanol and Carbon Dioxide

Figure 1 shows the DMC amount and BET surface area of the catalysts as functions of the calcination temperature of $ZrO_2 \cdot xH_2O$. The synthesis of DMC from methanol and CO_2 is reversible. The equilibrium level of the DMC amount is about 0.36 mmol at this reaction temperature, as reported previously (10). The DMC amount did not reach the equilibrium level under this reaction condition. The activity increased with the calcination temperature up to 673 K. The activity showed a maximum at 673 K, and then it decreased with the calcination temperature above

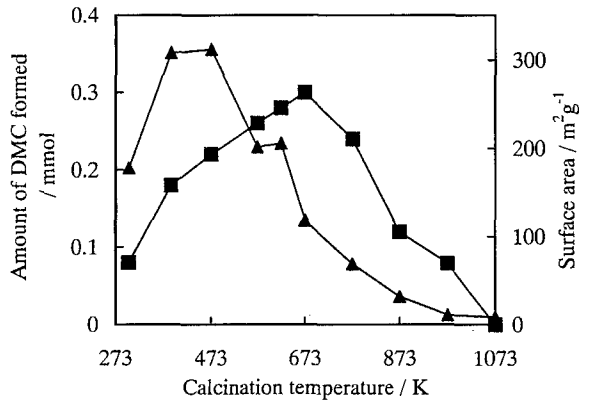

FIG. 1. The dependence of dimethyl carbonate formation (■) and surface area (▲) on the calcination temperature of zirconium hydroxide. Reaction conditions: 443 K, 2 h, $CH_3OH : CO_2 = 192 : 200$ mmol, and sample weight = 0.5 g. Surface area: BET method.

773 K. This indicated that the activity of DMC formation was very dependent on the calcination temperature. The BET surface area of the catalysts decreased with the calcination temperature. A clear relation between DMC formation and BET was not observed in Fig. 1.

Figure 2 shows the dependence of the amount of DMC formation over ZrO_2 calcined at 673 K on the reaction temperature. From a comparison of the results after 2 h of reaction, the DMC amount increased with the reaction temperature, reached a maximum at 443 K and then decreased above 443 K. DME was below the detection limit of the analysis in this temperature range. At 453 K, the DMC amount after 4 h of reaction was almost the same as after 2 h. The equilibrium level of DMC formation at 453 K should be about 0.30 mmol. On the other hand, the equilibrium level of DMC formation at 443 K was 0.36 mmol (10). After 16 h of reaction, the DMC amount formed at 413, 423, and 433 K was comparable to or beyond the DMC amount

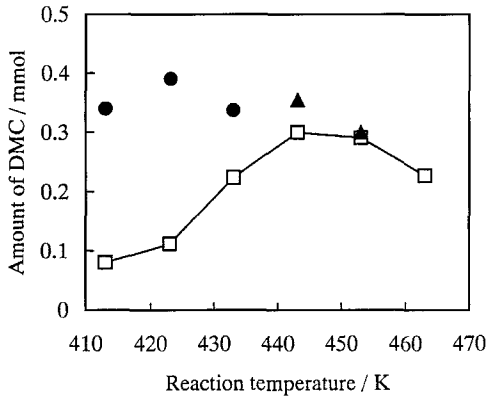

FIG. 2. The dependence of the amount of DMC formation on reaction temperature over ZrO_2 calcined at 673 K. Reaction time: 2 h (□); 4 h (▲); 16 h (●). Reaction conditions: $CH_3OH : CO_2 = 192 : 200$ mmol, and ZrO_2 weight = 0.5 g.

TABLE 1

Effect of the Amount of CO_2 Reactant on DMC Formation over the ZrO_2 Catalyst

Catalyst weight (g)	Reaction time (h)	Reactant (mmol)		Product (mmol)
		CO_2	CH_3OH	DMC
0.5	2	100	192	0.14
0.5	2	150	192	0.24
0.5	2	200	192	0.30
0.5	2	250	192	0.33
0.04[a]	16	250[a]	82	0.42

Note. ZrO_2 catalyst prepared by the calcination of zirconium hydroxide at 673 K. Reaction temperature: 443 K.

[a] The reaction was carried out in a stainless steel autoclave reactor with an inner volume of 30 ml.

formed at 443–463 K. From the results of the DMC amount at equilibrium, DMC formation from methanol and CO_2 seems to be exothermic. It was found that a lower reaction temperature is more favorable for greater DMC formation. In Fig. 2, DMC formation in the 2-h reaction is controlled by the formation rate at reaction temperatures lower than 453 K, and it is controlled by the reaction equilibrium at temperatures higher than 453 K.

The effect of the amount of CO_2 on DMC formation is listed in Table 1. Under this reaction condition, the DMC amount has not reached the equilibrium level. The DMC amount increased with the amount of CO_2, and the formation rate seemed to be almost proportional to the CO_2 amount. The reaction order with respect to CO_2 is almost one in the range of 100–200 mmol of CO_2. The DMC amount was at the saturation level with 250 mmol of CO_2. In addition, we carried out the reaction under another reaction condition as listed in Table 1. Under $CH_3OH : CO_2 = 82 : 250$ mmol at 443 K, 0.42 mmol of DMC was formed with 0.04 g of ZrO_2 catalyst (0.30 mmol of Zr) after 16 h. The DMC amount was higher than the total Zr amount in the ZrO_2 catalyst. This result is evidence that this reaction proceeded catalytically.

3.2. Catalyst Characterization by TGA, XRD, and LRS

Figure 3 shows the TGA and DTA profiles during the calcination of $ZrO_2 \cdot xH_2O$. Weight loss occurred in the range 298–673 K. The endothermic DTA peak was observed at 298–423 K. This behavior corresponds to the desorption of water. At 693–738 K, the exothermic DTA peak was observed with little weight loss. This seems to be assignable to the transition from a metastable tetragonal phase to a monoclinic phase of ZrO_2. In the catalyst preparation, the temperture was maintained for 3 h. The composition of the samples can be estimated by the results of the TGA profile, are listed in Table 2. All the water in $ZrO_2 \cdot xH_2O$ did not desorb when the sample was calcined at 623 and 673 K. On

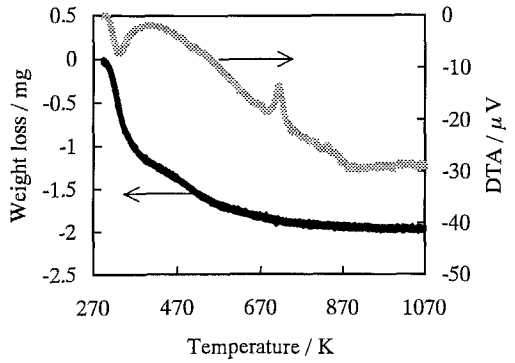

FIG. 3. TGA–DTA profile of $ZrO_2 \cdot xH_2O$. Heating rate = 6 K/min, Pt basket, air (20 ml/min), and sample weight = 11 mg.

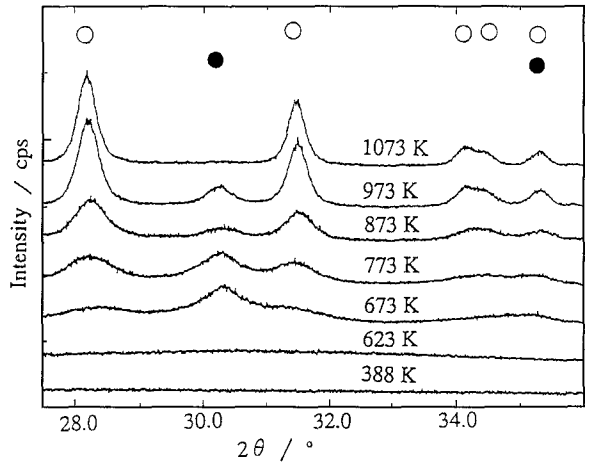

FIG. 4. XRD patterns of ZrO_2 prepared by calcination at various temperatures. Crystal structure: monoclinic (○); metastable tetragonal (●). X-ray source: Cu $K\alpha$.

the samples calcined above 773 K, the weight loss was almost the same. This indicated that stoichiometric ZrO_2 was formed. Strictly speaking, the samples at 623 and 673 K are not ZrO_2, but in this article these catalysts are also denoted as ZrO_2 for simplicity.

The crystal structure of ZrO_2 catalysts was investigated by XRD and the patterns are shown in Fig. 4. On the catalyst prepared by calcining below 623 K, clear diffraction peaks were not observed and the sample had an amorphous structure. On the samples calcined at 673 K, the broad peak due to a metastable tetragonal structure was observed, and the small peak due to a monoclinic structure was observed. At 773 K, peaks due to both metastable tetragonal and monoclinic structures were observed. At a higher calcination temperature, the monoclinic peak intensity increased and the tetragonal peak intensity decreased. The peak width on the sample calcined at 973 and 1073 K was small, and this indicated that the crystallite size was quite large, and this corresponds to low BET surface area as shown in Fig. 1.

Figure 5 shows the Raman spectra of the catalysts. It has been reported that the tetragonal phase of ZrO_2 exhibits typical Raman bands at 148, 263, 325, 472, 608, and 640 cm^{-1} and a strong peak is 263 cm^{-1} (11, 12). And the monoclinic phase of ZrO_2 exhibits bands at 140, 173, 185, 216, 260, 301, 328, 342, 378, 471, 499, 533, 553, 610, and 632 cm^{-1}. The strong peaks are at 173, 185, and 473 cm^{-1} (11, 12). In this case, the major phase was the monoclinic phase on the sample calcined above 673 K. The peak at 263 cm^{-1} is typical of the tetragonal phase, though a part of the signal can also

TABLE 2

Composition of the Sample Prepared by Calcining $ZrO_2 \cdot xH_2O$

Calcination temperature (K)	Weight loss (%)[a]	Catalyst composition[b]
623	15.8	$ZrO_2 \cdot 0.13H_2O$
673	16.5	$ZrO_2 \cdot 0.07H_2O$
773	17.5	ZrO_2
873	17.4	ZrO_2
973	17.5	ZrO_2
1073	17.3	ZrO_2

[a] (Weight loss/mg)/(Initial weight of $ZrO_2 \cdot xH_2O$/mg). Initial weight was about 11 mg.

[b] From the results of the samples calcined at 773–1073 K, the x value of $ZrO_2 \cdot xH_2O$ was calculated to be 1.44.

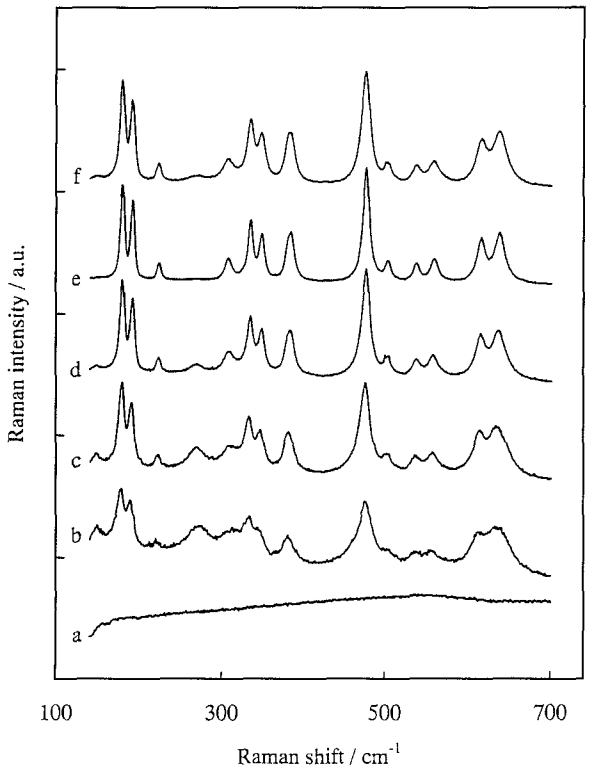

FIG. 5. Raman spectra of zirconia catalysts calcined at various temperatures. (a) 623 K; (b) 673 K; (c) 773 K; (d) 873 K; (e) 973 K; (f) 1073 K. Calcination: 3 h.

be due to the monoclinic phase. The small peak at 267 cm^{-1} was observed on the samples calcined at 673–873 K; its intensity decreased with calcination temperature. This behavior almost agrees with LRS and XRD results, but there are some different points. On the sample calcined at 973 K, the tetragonal phase was not found at all by LRS, but it was observed in XRD patterns. In the sample calcined at 673 K, the tetragonal phase seems to be the major phase from the XRD patterns, but the monoclinic phase seemed to be the major one from the LRS results. The ratio of these two phases is difficult to determine. Considering LRS is the near-surface sensitive method, these results indicate that the composition on the surface is different from that in the bulk. A similar tendency has been reported previously (11). In addition, it is suggested that the catalyst calcined at 623 K has an amorphous structure, since no clear peaks were observed at all with LRS and XRD.

3.3. *Characterization of Acid–Base Properties by TPD*

The results for the amount of single CO_2 and NH_3 adsorption are listed in Table 3. The amount of CO_2 adsorption increased little in the calcination temperature range of 573–673 K, and it decreased above 673 K. The amount of NH_3 adsorption decreased with the calcination temperature. It has been reported that surface acid and base properties are very dependent on the pretreatment temperature (13). To investigate the acid–base properties on various ZrO_2 catalysts in detail, a TPD experiment was carried out. Figure 6 shows a TPD profile of CO_2 adsorbed on ZrO_2 calcined at various temperatures. CO_2 was desorbed in a wide temperature range. Ripples on the TPD profile in a lower temperature range were caused by the response gap of an electrical furnace from programmed proportional heating. The amount of desorbed CO_2 from zirconia calcined at 573 K was quite large, but the desorption amount in a higher temperature range was quite small. On one hand, this indicated that the sample had little strong basicity. On the other hand, quite a large number of strong basicsites are formed on the surface by calcination at 673 K. The number of stronger basic sites decreased with increases in the calcination temperature above 673 K. Figure 7 shows the TPD profiles of

TABLE 3

Adsorption Amount of CO_2 and NH_3 on Zirconia Catalysts

Calcination temperature (K)	CO_2 (mmol 0.5 g-cat^{-1})	NH_3 (mmol 0.5 g-cat^{-1})
573	0.17	0.32
623	0.18	0.26
673	0.20	0.26
773	0.10	0.16
873	0.07	0.10

Note. Irreversible adsorption amount measured by the volumetric method at room temperature.

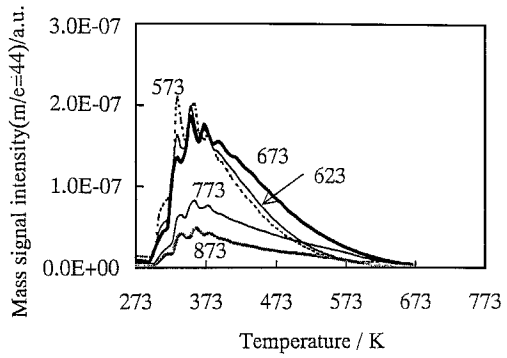

FIG. 6. Profile of temperature-programmed desorption of CO_2 adsorbed on zirconium oxides prepared by the calcination of zirconium hydroxide at 573–873 K. The calcination temperature is described in the figure. CO_2 adsorption: $P_{CO_2} = 6.6$ kPa and 293 K. TPD conditions: heating rate = 7 K/min and sample weight = 0.05 g.

NH_3 adsorbed on zirconia. The distribution of acid strength seems to be similar, though the amount decreased with the calcination temperature.

Figure 8 shows the TPD profiles of CO_2 (Fig. 8a) and NH_3 (Fig. 8b) from ZrO_2 with $CO_2 + NH_3$ coadsorption. $CO_2 + NH_3$ represents the CO_2 adsorption procedure followed by the NH_3 adsorption procedure. Figure 9 shows the TPD profiles of CO_2 (Fig. 9a) and NH_3 (Fig. 9b) from ZrO_2 with $NH_3 + CO_2$ coadsorption. On ZrO_2 calcined at 673 K, the shoulder peak near 500 K was observed in these four TPD profiles. Similar peaks were observed on the zirconia calcined at 873 K, but the area of this shoulder peak is much smaller than that on the catalyst calcined at 673 K. On zirconia calcined at 573 K, the shoulder peak was not observed clearly under various adsorption conditions. From a comparison of (a) and (b) in Figs. 8 and 9, the shoulder peaks of CO_2 and NH_3 were observed in almost the same temperature range. This indicated interaction between adsorbed CO_2 and NH_3, and these peaks have been assigned

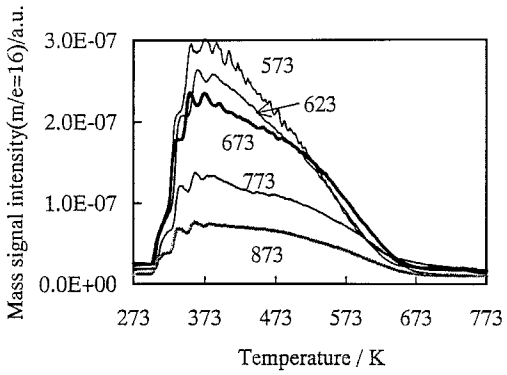

FIG. 7. Profile of temperature-programmed desorption of NH_3 adsorbed on zirconium oxides prepared by the calcination of zirconium hydroxide at 573–873 K. The calcination temperature is described in the figure. NH_3 adsorption: $P_{NH_3} = 6.6$ kPa and 293 K. TPD conditions: heating rate = 7 K/min and sample weight = 0.05 g.

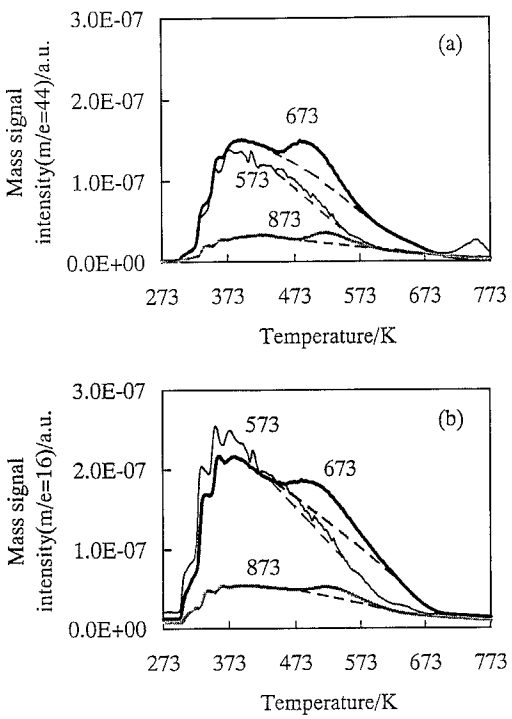

FIG. 8. Profiles of temperature-programmed desorption of CO_2 (a) and NH_3 (b) from $CO_2 + NH_3$ coadsorbed on zirconium oxides prepared by the calcination of zirconium hydroxide at 573, 673, and 873 K. Calcination temperature: 573 K (thin black line), 673 K (bold black line), and 873 K (bold gray line). CO_2 and NH_3 adsorption: $P_{CO_2} = P_{NH_3} = 6.6$ kPa, 293 K, and NH_3 adsorption after CO_2 adsorption. TPD conditions: heating rate = 7 K/min and sample weight = 0.05 g.

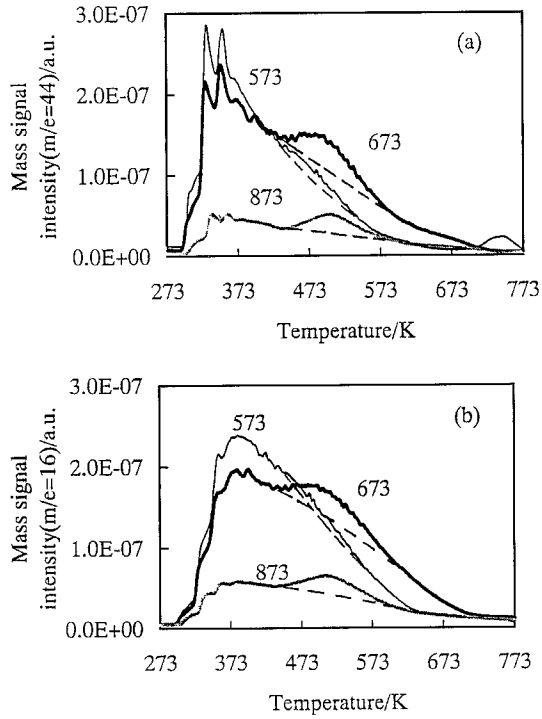

FIG. 9. Profiles of temperature-programmed desorption of CO_2 (a) and NH_3 (b) from $NH_3 + CO_2$ coadsorbed on zirconium oxides prepared by the calcination of zirconium hydroxide at 573, 673, and 873 K. Calcination temperature: 573 K (thin black line), 673 K (bold black line), and 873 K (bold gray line). NH_3 and CO_2 adsorption: $P_{CO_2} = P_{NH_3} = 6.6$ kPa, 293 K, and CO_2 adsorption after NH_3 adsorption. TPD conditions: heating rate = 7 K/min and sample weight = 0.05 g.

to the desorption from neighboring acidic and basic sites as reported previously (14). The amount of the shoulder peak was estimated by comparing between the TPD profiles of single adsorption and coadsorption. The estimate is described with a broken line in Figs. 8 and 9. The results are listed in Table 4. On one hand, the total amount of desorption was influenced by the order of gas introduction, especially in a lower temperature range. On the other hand, the amount in a higher desorption temperature range was not dependent on the order of gas introduction. From Table 4, the molar ratio of CO_2 to NH_3 in a higher desorption temperature range was about 1. These results suggest that the interaction between CO_2 and NH_3 is 1 : 1 and stabilizes the adsorption state. It seems that the catalyst calcined

TABLE 4

Desorption Amount of CO_2 and NH_3 in TPD Experiments

Calcination temperature (K)	Temperature range of desorption profile (K)	CO_2	NH_3	Adsorbate: $CO_2 + NH_3$[a]		$NH_3 + CO_2$[b]	
		Desorbed species (mmol 0.5 g-cat^{-1}):					
		CO_2	NH_3	CO_2	NH_3	CO_2	NH_3
573	300–700	0.17	0.30	0.15	0.24	0.23	0.22
573	430–600			0.006	0.008	0.006	0.005
673	300–700	0.20	0.26	0.16	0.26	0.27	0.23
673	430–600			0.017	0.021	0.020	0.019
873	300–700	0.07	0.10	0.07	0.08	0.09	0.08
873	430–600			0.006	0.005	0.009	0.010

[a] CO_2 adsorption before NH_3 adsorption.
[b] NH_3 adsorption before CO_2 adsorption.

at 673 K has more acid–base sites than two other catalysts. This behavior can explain the activity of DMC formation more clearly than that in the single adsorption experiments. This suggests that the active site of DMC formation is the neighboring acid–base site.

Assuming that this neighboring acid–base site is the active site on ZrO_2 calcined at 673 K, the number of active sites is 0.02 mmol/0.5 g ZrO_2, as shown in Table 4. On the other hand, the amount of DMC formation shown with the closed triangle in Fig. 2 is 0.36 mmol/0.5 g of ZrO_2. This corresponds to the turnover number (TON) = 0.36/0.02 = 18. In another case, even if all of the CO_2 adsorption sites may be active, the number is 0.20 mmol/0.5 g of ZrO_2, listed in Table 3. This corresponds to TON = 0.36/0.20 = 1.8. Under other reaction conditions, 0.42 mmol of DMC was formed using 0.04 g of ZrO_2 (Table 1). If the neighboring acid–base site is the active site, the number of active sites is 1.6×10^{-3} mmol/0.04 g of ZrO_2. The TON of DMC formation can be estimated to be about 260 ($=0.42/(1.6 \times 10^{-3})$). And even if the activesites are all of the CO_2 adsorption sites, the number of sites is 0.016 mmol/0.04 g ZrO_2; the TON can be estimated to be 26 (=0.42/0.016). These results and discussion show that DMC was synthesized catalytically.

3.4. *FTIR Observation of Adsorbed CO_2 and CH_3OH*

Figure 10 shows the DRIFT spectra of methanol adsorption and CO_2 introduction at 443 K on ZrO_2 calcined at 673 K. When methanol was introduced into the sample, peaks appeared at 1160 and 1054 cm^{-1}; these are assigned to the C–O stretching modes of monodentate and bidentate methoxy species, respectively (15, 16). When CO_2 was introduced into the catalyst with methanol adsorption, the 1160-cm^{-1} peak decreased and the peaks at 1600, 1474, 1370, 1200, and 1112 cm^{-1} increased. The change in peak intensities became significant with CO_2 pressure. These peaks can be assigned to the methoxy carbonate species. The methoxy carbonate species on the surface of alumina has already been observed (17). The peak intensity at 1050 cm^{-1} did not change with CO_2 pressure. These results indicated that the methoxy carbonate species is easily formed from the reaction of CO_2 with adsorbed monodentate methoxy species, and the formation was more favorable under higher CO_2 pressures. This agrees with the dependence of the CO_2 pressure on the activity, as shown in Table 1. It is suggested that the methoxy carbonate species is the reaction intermediate. Figure 11 shows the DRIFT spectra of CO_2 adsorption and methonol introduction. The peaks at 1620, 1575, 1430, 1330, and 1220 cm^{-1} were observed on CO_2 adsorption. The peaks at 1620, 1430, and 1220 cm^{-1} can be assigned to the bicarbonate species, and the peaks at 1575 and 1330 cm^{-1} can be assigned to the bidentate carbonate species (18–20). The bicarbonate species was the main one observed under both low and high CO_2 pressure. As CO_2 was purged with He, the total peak area of CO_2 adsorption decreased. The bicarbonate peaks decreased and bidentate carbonate increased in this case. After methanol was introduced into the sample with CO_2 adsorption, the spectrum was very similar to that of methanol adsorption on the ZrO_2 surface without preadsorption. The methoxy

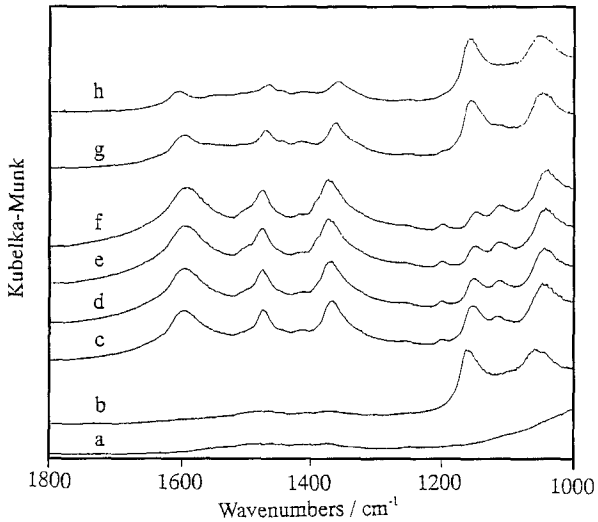

FIG. 10. DRIFT spectra of methanol and CO_2 adsorption on ZrO_2 calcined at 673 K: (a) after pretreatment; (b) CH_3OH; (c) CO_2, 0.1 MPa; (d) CO_2, 1.0 MPa; (e) CO_2, 3.0 MPa; (f) CO_2, 5.0 MPa; (g) He, 0.1 MPa; (h) CH_3OH. Pretreatment: 673 K for 0.5 h and He flow. Adsorption temperature of methanol and CO_2: 443 K.

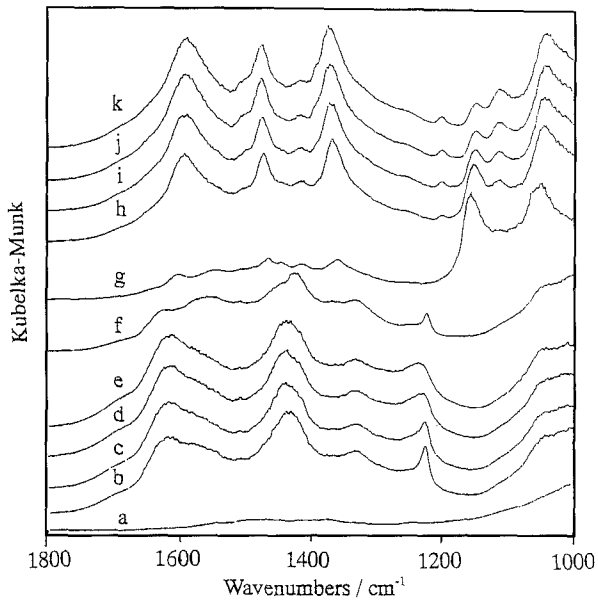

FIG. 11. DRIFT spectra of CO_2 and methanol adsorption on ZrO_2 calcined at 673 K: (a) after pretreatment; (b) CO_2, 0.1 MPa; (c) CO_2, 1.0 MPa; (d) CO_2, 3.0 MPa; (e) CO_2, 5.0 MPa; (f) He, 0.1 MPa; (g) CH_3OH; (h) CO_2, 0.1 MPa; (i) CO_2, 1.0 MPa; (j) CO_2, 3.0 MPa; (k) CO_2, 5.0 MPa. Pretreatment: 673 K for 0.5 h and He flow. Adsorption temperature of CO_2 and methanol: 443 K.

carbonate species was at a very low level. From a comparison between Figs. 10 and 11, it is found that the methoxy carbonate species is formed by the reaction between adsorbed methoxy species and CO_2 more easily than by the reaction between adsorbed CO_2 and methanol. This is probably because methanol can desorb CO_2 adsorbed on the surface. This suggests that the interaction between methanol and the surface is stronger than that between CO_2 and the surface. Next, CO_2 was introduced again; methoxy carbonate was formed just as in Figure 10.

Considering that methoxy carbonate reacts with methanol to form DMC and OH^-, methoxy carbonate is the reaction intermediate. The methoxy carbonate species is present on the basic site on the catalyst surface. Furthermore, methanol should be activated to $CH_3^{\delta+}$–$OH^{\delta-}$ on the neighboring acidic site. The reaction scheme of DMC synthesis from methanol and CO_2 is described below:

$$CH_3OH \rightarrow CH_3O^-(a) + H^+(a) \quad \text{(Basic site)} \quad [7]$$

$$CO_2 \rightarrow CO_2(a) \quad \text{(Basic site)} \quad [8]$$

$$CH_3O^-(a) + CO_2(a) \rightarrow CH_3OCO_2^-(a) \quad \text{(Basic site)} \quad [9]$$

$$CH_3OH \rightarrow CH_3^+(a) + OH^-(a) \quad \text{(Acidic site)} \quad [10]$$

$$CH_3OCO_2^-(a) + CH_3^+(a) \rightarrow (CH_3O)_2CO \quad [11]$$

$$H^+ + OH^- \rightarrow H_2O. \quad [12]$$

The elementary reaction [10] or [11], which is related to the activation of methanol on the acidic site, may be the rate-determining step in DMC formation. It is suggested that high selectivity of DMC formation on the catalyst is probably due to rapid conversion of the methoxy species to the methoxy carbonate species [9] under high CO_2 pressure.

From the Raman study, it was found that more tetragonal phase is present on the surface of ZrO_2 calcined at 673 K than on the surfaces of other ZrO_2 catalysts. It is suggested that the tetragonal phase is more effective for acid–base bifunction and DMC synthesis from methanol and CO_2.

4. CONCLUSION

(1) ZrO_2 catalyzed the direct synthesis of dimethyl carbonate from methanol and CO_2.

(2) The DMC formation rate was highly dependent on the structure of ZrO_2. On zirconia prepared by the calcination of zirconium hydroxide at 673 K, whose surface consisted of a major monoclinic phase and a minor tetragonal phase, the highest rate of DMC formation was observed.

(3) TPD of coadsorbed CO_2 and NH_3 suggested that a neighboring acid–base site is present on ZrO_2. The amount of the site seems to correspond to the activity of DMC formation, and this suggests that the neighboring acid–base site on the tetragonal ZrO_2 surface is active for DMC formation.

(4) The methoxy carbonate species was easily formed on ZrO_2 calcined at 673 K by the reaction between the monodentate methoxy species and CO_2. It is suggested that the methoxy carbonate species is thought to be the reaction intermeditate of DMC synthesis on ZrO_2, and this causes high selectivity of DMC formation.

ACKNOWLEDGMENT

A part of this research was supported by the International Joint Research Project "Agrofuel" from the New Energy and Industrial Technology Development Organization (NEDO) of Japan.

REFERENCES

1. Ono, Y., *Appl. Catal. A* **155**, 133 (1997).
2. Pacheco, M. A., and Marshall, C. L., *Energy Fuels* **11**, 2 (1997).
3. Romano, U., Tesei, R., Mauri, M. M., and Rebora, P., *Ind. Eng. Chem. Prod. Res. Dev.* **19**, 396 (1980).
4. Molzahn, D., Jones, M. E., Hartwell, G. E., and Puga, J., U.S. Patent 5,387,708, 1995.
5. King, S. S. T., Jones, M. E., and Olken, M. M., U.S. Patent 5,391,803, 1995.
6. Matsuzaki, T., and Nakamura, A., *Catal. Surv. Jpn.* **1**, 77 (1997).
7. Fang, S., and Fujimoto, K., *Appl. Catal. A* **142**, L1 (1996).
8. Kizkink, J., *Collect. Czech. Chem. Commun.* **58**, 1399 (1993).
9. Kizlink, J., and Pastucha, I., *Collect. Czech. Chem. Commun.* **60**, 687 (1995).
10. Tomishige, K., Sakaihori, T., Ikeda, Y., and Fujimoto, K., *Catal. Lett.* **58**, 225 (1999).
11. Yamamoto, T., Tanaka, T., Takenaka, S., Yoshida, S., Onari, T., Takahashi, Y., Kosaka, T., Hasegawa, S., and Kudo, M., *J. Phys. Chem. B* **103**, 2385 (1999).
12. Mercera, P. D. L., van Ommen, J. G., Doesburg, E. B. M., Burggraaf, A. J., and Ross, J. R. H., *Appl. Catal.* **57**, 127 (1990).
13. Nakano, Y., Iizuka, T., Hattori, H., and Tanabe, K., *J. Catal.* **57**, 1 (1978).
14. Xu, B.-Q., Yamaguchi, T., and Tanabe, K., *Chem. Lett.* 1663 (1988).
15. Bensitel, M., Moravek, V., Lamotte, J., Saur, O., and Lavalley, J.-C., *Spectrochem. Acta Part A* **43**, 1487 (1987).
16. Montagne, X., Lynch, J., Freund, E., Lamotte, J., and Lavalley, J. C., *J. Chem. Soc. Faraday Trans. 1* **83**, 417 (1987).
17. Lamotte, J., Saur, O., Lavalley, J. C., Busca, G., and Lorezelli, C., *J. Chem. Soc. Faraday Trans. 1* **82**, 3019 (1986).
18. Dang, Z., Anderson, B. G., Amenoniya, Y., and Morrow, B. A., *J. Phys. Chem.* **99**, 14437 (1995).
19. Hertl, W., *Langmuir* **5**, 96 (1989).
20. Bianchi, D., Chafik, T., Khalfallah, M., and Teichner, S. J., *Appl. Catal.* **112**, 219 (1994).